Experiments on Enhancing the Particle Charging Performance of an Electrostatic Precipitator

Chenghang Zheng, Dawei Duan, Qianyun Chang, Shaojun Liu, Zhengda Yang, Xintao Liu, Weiguo Weng, Xiang Gao[*]

State Key Lab of Clean Energy Utilization, State Environmental Protection Engineering Center for Coal-Fired Air Pollution Control, Zhejiang University, Hangzhou 310027, China

ABSTRACT

Particle charging is an essential process for electrostatic precipitators (ESPs) in removing particles. A particle charge measurement system, which can adjust the flue gas temperature, was designed to study the effects of the flue gas parameters (viz., temperature and humidity), particle composition, and discharge electrodes on particle charging. The particle charge increased with the temperature when the applied electric field strength was constant. For particles with a diameter of 0.73 μm, the average charge increased by 30% (from 140 e to 183 e) when the temperature increased from 300 K to 363 K. Furthermore, with a constant electric field strength of –4.2 kV cm^{-1}, the average charge increased by 98% when the relative dielectric constant increased from 4.5 to 11.8. Increased relative humidity significantly accelerated particle charging. For particles > 0.1 μm, the average charge increased by more than 50% when the relative humidity increased from 30% to 80%. Optimizing the discharge electrode also enhanced charging. After the wire electrode (d = 1 mm) was replaced by a ribbon electrode, particle charging increased by more than 75% for 0.7 μm particles at –4.2 kV cm^{-1}.

Keywords: Particle charging; Temperature; Humidity; Discharge electrode; Relative dielectric constant.

INTRODUCTION

The global consumption of coal by the power sector is estimated to increase over the next two decades (ExxonMobil, 2017). In China, nearly 50% of coal is consumed in coal-fired power plants (Wang *et al.*, 2015). Many pollutants, such as NO$_x$ and SO$_x$, are generated during the coal combustion process (Hu *et al.*, 2017; Yang *et al.*, 2018b, c; Wang *et al.*, 2019; Zheng *et al.*, 2019). Among pollutants, particulate matter (PM) can result in potential visibility problems and adverse effects on human health (Crilley *et al.*, 2014; Kim *et al.*, 2015; Yang *et al.*, 2017; Lin *et al.*, 2018; Zheng *et al.*, 2018; Li *et al.*, 2019; Zhou *et al.*, 2019). Therefore, developing technology to control PM emission is essential.

The electrostatic precipitator (ESP) is a well-known, highly efficient device for cleaning exhaust gases from industrial processes (Wang *et al.*, 2015; Sun *et al.*, 2018; Yang *et al.*, 2018a). The overall mass-based collection efficiencies of ESPs can exceed 99% (Xu *et al.*, 2016a, b). However, a decrease in collection efficiency was observed for different kinds of particles with the reduction in particle size to between 0.1–l μm (Zhuang *et al.*, 2000). One important reason for the decrease is the low charging efficiency of fine particles (Lawless, 1996). Studying the charging mechanism of particles is useful for enhancing the charging efficiency. Different numerical techniques, theoretical models, and experiments have been proposed and developed to elucidate the charging mechanism of particles.

Numerical techniques have been adopted by researchers to analyze particle charging to model unipolar chargers. The Monte Carlo simulation was developed to capture the charging characteristics of particles with complex shapes (Biskos *et al.*, 2004). Apart from the Monte Carlo simulations of theoretical charging processes, numerical techniques were also developed to analyze the charging process in unipolar chargers. A 2D numerical model was developed to predict the charging process in real unipolar chargers with complex geometries, which contain the fully coupled calculation of the flow, electric potential, and ion concentration fields and the charging dynamics of particles (Chien *et al.*, 2011; Chien and Tsai, 2013). In the aspect of theoretical models, a non-spherical particle charging model for particles of all sizes and a charge distribution model for particles sized 0.01–10 μm were developed in recent years (Gopalakrishnan *et al.*, 2013; Domat *et al.*, 2014). Many measurements of electric charges were developed to confirm the validity of the field charging model. Frank *et al.* (2004) measured the electric

---

[*] Corresponding author.
  Tel.: +86-571-87951335; Fax: +86-571-87951616
  E-mail address: xgao1@zju.edu.cn

charge on droplet particles sized 0.1–20 µm by using three different methods. The average charges were fairly consistent with the prediction of the combined charging model of Lawless (1996). Long and Yao (2010) analyzed different kinds of charging models in the continuum regime and compared their data with the experimental data (Hewitt, 1957), which indicated that the model established by Lawless should be the first choice for modeling the particle charging dynamics in ESPs. The effect of the dielectric constant of materials on the unipolar diffusion charging of nanoparticles was also investigated (Shin *et al.*, 2009). Xu *et al.* (2009) investigated the effect of power supply with different frequencies and different particle flow rates on particle charging. Park *et al.* (2011) used multichannel chargers to demonstrate that increasing ion concentration is an important factor in increasing the average charge of the particles. Another new charger (Alonso and Huang, 2015) was also designed to enhance the nanoparticle charge.

Although many experiments were conducted, most of them mainly focused on the effects of the charge devices, particle sizes, and ion concentrations on the particle. How to adjust the actual operating conditions of the ESP and the main particle component to enhance the particle charge is unclear (Zheng *et al.*, 2016). In this research, a particle charge measurement system was designed to study the effects of particle properties, flue gas parameters, and discharge electrodes on particle charge. The temperature varied from 293 K to 383 K, and the range of relative humidity was 0–100%, which were aimed at how to improve the efficiency of ESP under real operating conditions. The effects of different discharge electrodes, including ribbon electrode, sawtooth electrode, screw electrode, and two wire electrodes (d = 1, 3 mm), on particle charge were compared. Six types of particles, namely, power plant fly ash (Ash A), coal pyrolysis furnace fly ash (Ash B), glass bead (Particle C), silica (Particle D), aluminum oxide (Particle E), and calcium oxide (Particle F), were investigated. This research mainly aimed to study how the main particle component, flue gas parameters, and discharge electrodes influence the charging mechanism of particles and to obtain the method of enhancing the particle charge.

EXPERIMENTAL SETUP AND METHODS

A schematic of the experimental system is shown in Fig. 1. The system consisted of five parts, namely, a gas-controlled system, particle feeders, a particle charging device, a high-voltage power supply, and a particle charge measurement system.

The gas-controlled system consisted of a fan, a buffer vessel, an electric heater, and a rotameter. The main stream of simulated flue gas was produced by a draught fan from the air with a maximum flow rate of 70 L min^{-1} during the experiments. The buffer vessel was a cylindrical metal barrel, with a diameter of 20 cm and a height of 40 cm, connected to the middle of the pipeline linked to the feeder and the charging system. This configuration prevented excess particles from depositing in and blocking the pipes and aimed to adjust the flow rate. The relative humidity of

the gas, which ranged from 0% to 100%, was measured by an electronic hygrometer (CX309; Anseny, Ltd., China). The gas temperature was controlled in the range of 293 K to 383 K by an electric heater. The temperature of these experiments was generally 313 K, apart from the experiments aimed at exploring particle charging characteristics at different temperatures. All pipes were covered with thermal insulation material to reduce undesired heat loss. In addition, the designed pipelines in were as straight and short as possible to reduce the mass loss. Then, the gas entered the charging system. The charging time varied in the range of 0.06–0.1 s by changing the gas flow rate using the rotameter. Afterward, the particle charge and concentration were measured at the outlet of the particle charging system. The measurement was taken when each experiment was adjusted to a stable condition as the experiment required. The time of each experiment was very short, usually within 2 minutes.

Six types of particles, namely, power plant fly ash (Ash A), coal pyrolysis furnace fly ash (Ash B), glass bead (Particle C), silica (Particle D), aluminum oxide (Particle E), and calcium oxide (Particle F), were used to study the charging characteristic of different particles. The experimental particle mass concentration and the number concentration were approximately 120 mg m^{-3} and 190,000 # cm^{-3}, respectively. The experimental particles of these experiments were generally power plant fly ash, apart from the experiments aimed at exploring effect of the main particle component on particle charging. The particles were injected into the simulated flue gas by an electromagnetic vibrating feeder, which was self-designed and consisted of four springs and an electromagnet system. When the electromagnet was magnetized, the springs would be extruded and the base of the spring moved downward. The particles moved forward with the vibration of the base, then entered the inlet of the pipes through the connecting tube. The feeding rate could be adjusted in accordance with the vibration frequency of the vibration controller, of which the vibration frequency range was 0–100 Hz. The particle feeder was replaced by an aerosol generator (Condensation Monodisperse Aerosol Generator Model 3475; TSI Inc., USA) to study the particle charging characteristics at different temperatures. It can produce polydisperse aerosol particles with an average particle size of 0.1–8 µm, which are almost electrically neutral. The material it generated was bis(2-ethylhexyl) sebacate (DEHS) aerosol particles, which were generated by the DEHS vapor condensing on the sodium chloride crystal nucleus. In this research, the total mass and number concentration of the generated aerosol particles was approximately 120 mg m^{-3} and 233,843 # cm^{-3}, respectively, which were controlled by adjusting the nitrogen pressure, saturator flow valve, temperature, and reheater temperature.

The particle charging device was a wire-plate discharge configuration with a negative direct current power supply (TRC2020; Teslaman Electronics Co., Ltd., China). The wire-plate negative corona discharge device, which was made of plexiglass (600 mm long, 200 mm wide, and 100 mm high), consisted of a wire discharge electrode and
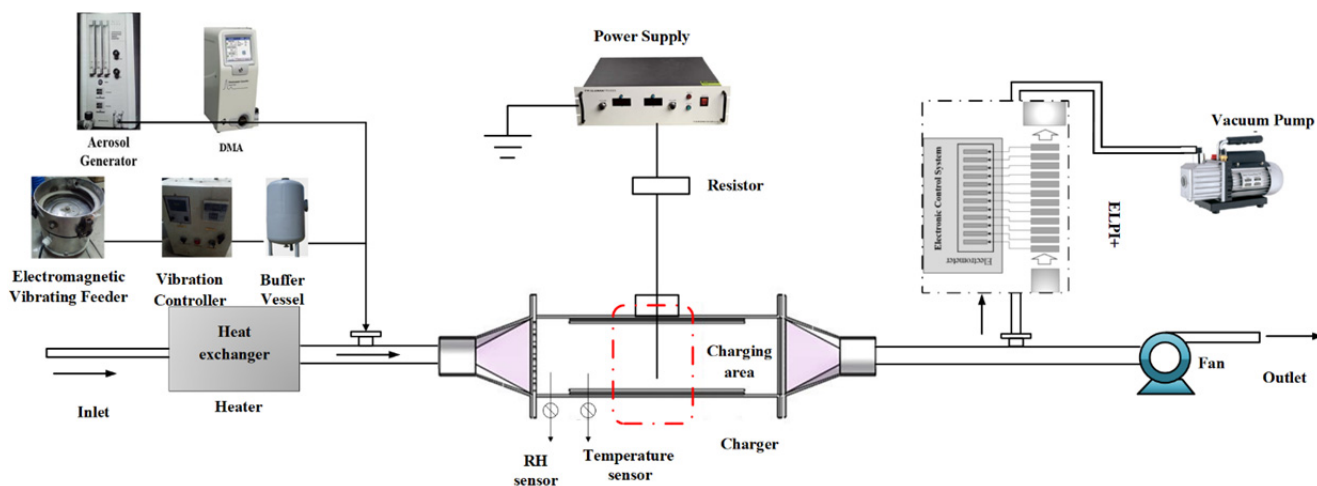
(a) The particle charge measurement system.
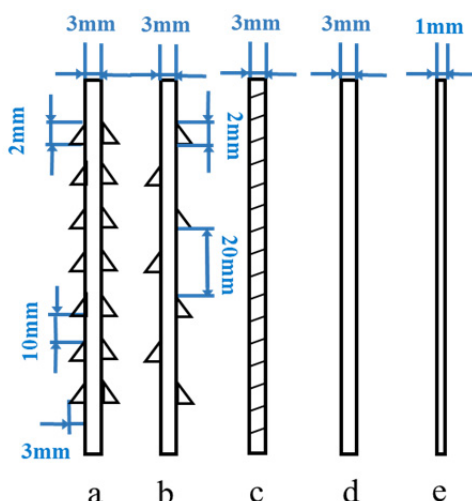
a: ribbon electrode; b: sawtooth electrode; c: screw electrode; d: wire electrode (3 mm); e: wire electrode (1 mm).
(b) Geometry of discharge electrodes2

Fig. 1. Schematic of the experimental system.

two grounded plates. The plates were cleaned after finishing several experiments to avoid the influence of precipitated aerosol. Ribbon electrode, sawtooth electrode, screw electrode, and two wire electrodes with diameters of 1 and 3 mm were used as the discharge electrodes (as shown in Fig. 1). The ribbon electrode was generally used as the discharge electrode, apart from the experiments aimed at exploring the effect of electrodes on particle charge. The discharge electrodes were 200 mm long, and the discharge gap was 50 mm. The length of the corona discharge region was 60 mm. The charging time was generally 0.1 s, while the charging time of the experiments aimed at effect of dielectric constant was 0.06 s. The charging time set can minimize the deposition of particles while ensuring sufficient charging time (Long and Yao, 2010). The negative high voltage generated by the negative power supply with a range of 0–30 kV was applied to the discharge electrode.

The particle measurement system consisted of an electrostatic low-pressure impactor (ELPI+; Dekati, Ltd.,

Finland), a vacuum pump (SV25B; Ernst Leybold, Ltd., Germany), and a sampling probe. The inside of the sampling probe was technically coated to prevent electrostatic adsorption, which can minimize the loss of small particles. Using the vacuum pump, the flue gas was sampled through the sampling probe at a flow rate of 10 L min^{-1}. The particle charge and number concentration of particles of different sizes were obtained by the ELPI+. The measured size range of the particles was 0.006–10 μm, and these particles were classified into 14 stages. The particle number concentration of each stage was obtained by detecting the signal of the induced current.

The particle number concentration was calculated using the fractional current resulting from the continuous deposition of charged particles on each aluminum/polycarbonate foil. As expressed in Eq. (1), the ELPI+ will automatically convert the measured current into the fractional concentration of the particles:

$$I = PneQN \tag{1}$$

where I is the fractional current, N is the fractional number concentration of particles, P is the fractional efficiency of particle charging, n is the number of elementary charges carried by the particle, e is the elementary charge (1.602×10^{-19} C), and Q is the sampling flow rate (10 L min^{-1}). The power plant fly ash size distribution measured by the ELPI+ is shown in Fig. 2.

After closing the charger of the ELPI+, the charge of a particle was calculated using the signal of the fractional induced current of the ELPI+. For each experiment, n is calculated using Eq. (2):

$$n_1 = \frac{I_1}{Q_1 \times n \times e} \tag{2}$$

where n_1 is the number of elementary charges carried by a particle, I_1 is the signal of the fractional induced current of the ELPI+ (A), Q_1 is the sampling flow rate (cm^3 s^{-1}), N is the particle number concentration (cm^{-3}), and e is the elementary charge (1.602×10^{-19} C).

RESULTS AND DISCUSSION

Particle Charging Characteristics at Different Temperatures

Fig. 3 shows the effect of temperature on particle charge at -4.4 kV cm^{-1}. The particle charge increased with increasing temperature and particle size. For the particles 0.73 µm in size, the average particle charge was increased by 30% from 140 e to 183 e when the temperature increased from 300 K to 363 K. Particle charge increased with increasing temperature (Fig. 4). With high applied electric field strength, the enhancement of particle charge with rising temperature was rapid. When the average applied electric field strength was -6.0 kV cm^{-1}, the particle charge increased
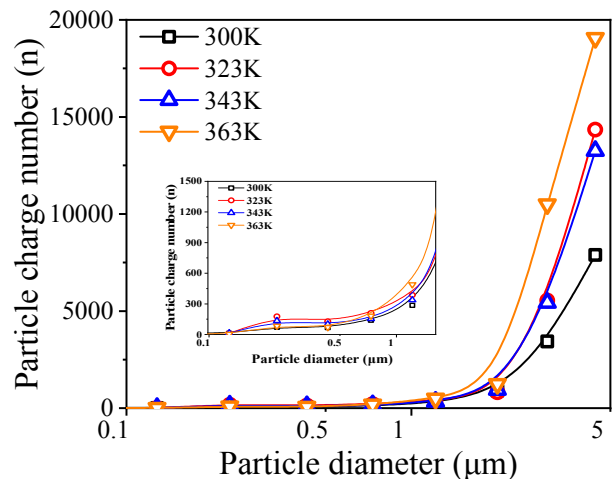

Fig. 3. Effect of temperature on particle.

from 1.8×10^4 e to 4.3×10^4 e, with the temperature increasing from 300 K to 363 K. By contrast, when the average applied electric field strength was -6.4 kV cm^{-1}, the particle charge increased from 1.8×10^4 e to 6.4×10^4 e, with the temperature increasing from 300 K to 363 K; the increment was more than that at the average applied electric field strength of -6.0 kV cm^{-1}. High temperature led to an increase in the mean free path of the surrounding gas molecules. A larger mean free path leads to more energy gained by an electron when it is accelerated in the applied electric field before colliding with a background molecule. The electron energy and probability of the gas molecule to be ionized increased with increasing mean free path (Hamou *et al.*, 2013), such that the number of ions and the discharge current increased (as shown in Fig. 5). Therefore, the high temperature accelerated the particle charge at the same applied voltage.
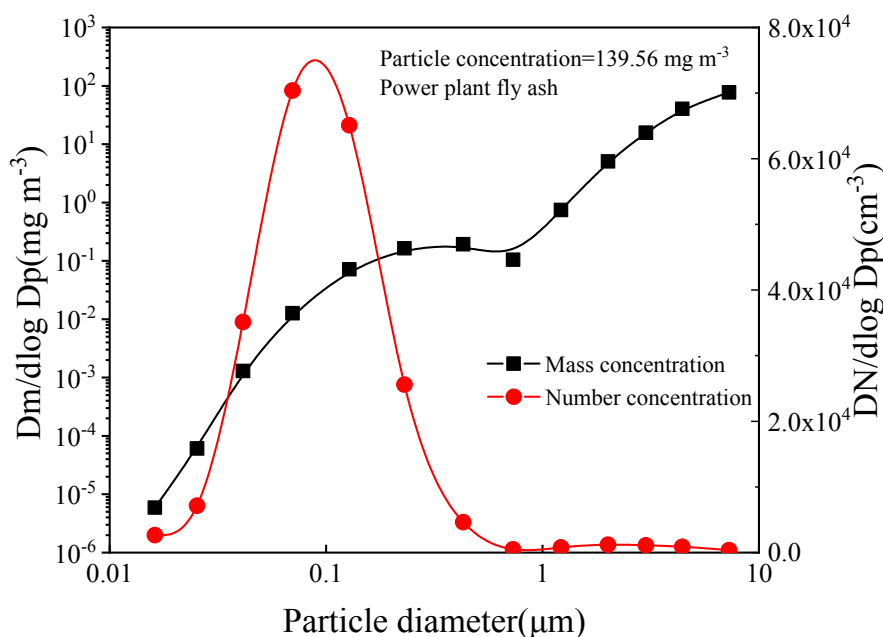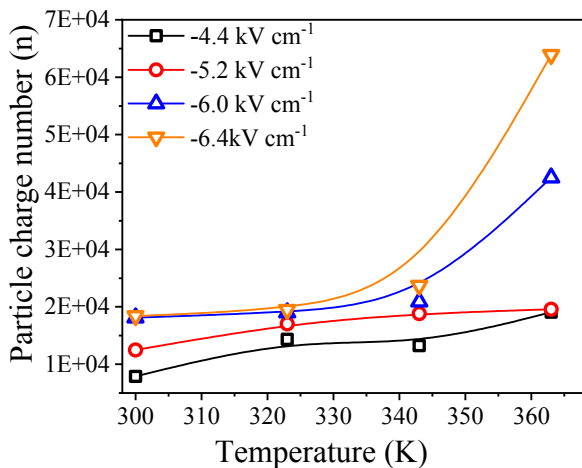

Fig. 2. Power plant fly ash size distribution.

Fig. 4. Effect of temperature on particle charge at different applied voltages.

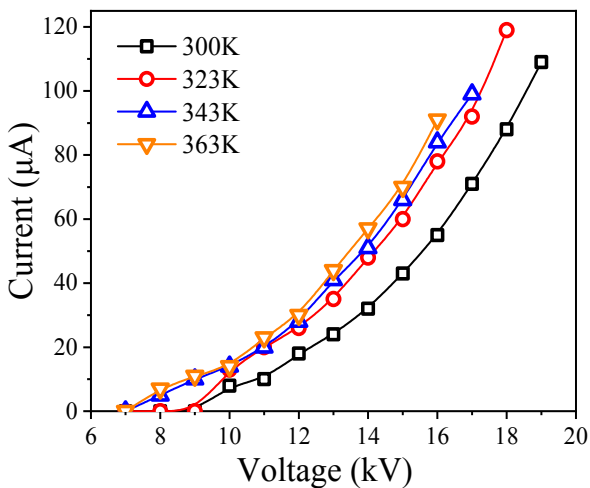**Fig. 6.** Effect of temperature on particle charge at maximum applied voltages.

Fig. 5. I–V characteristics curve in different temperatures.

Fig. 6 shows the effect of temperature on particle charge at maximum applied voltages. For corona discharges above 323 K, the particle charge decreased with increasing temperature. The maximum applied voltage (Ghaleb *et al.*, 2008; Ghaleb and Belasri, 2012), electric field strength, and ion concentration in the corona discharge region decreased with increasing temperature. Hence, the movement of ions to the surface of the particles and the collision frequency decreased, thereby resulting in a corresponding decrease in the particle charge. For 293 K to 323 K, the particle charge at 323 K was slightly higher than that at 293 K because the decrease in the maximum operating voltage was small. However, the accelerating effect of temperature on corona discharge was obvious. Therefore, the discharge current at 323 K was slightly higher than that at 293 K. The ion concentration also increased. For particles smaller than 0.5 μm, diffusion charging was stronger than field charging (Jaworek *et al.*, 2007). With the increase of temperature, the diffusion charging will be much stronger. Therefore, the charge of particles less than 0.5 μm at 323 K was higher than that at 293 K.
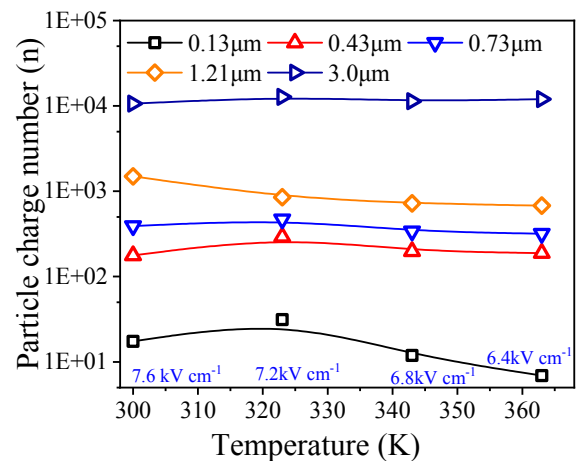
Effect of the Main Particle Component on Particle Charging

In this research, six types of particles, namely, power plant fly ash (Ash A), coal pyrolysis furnace fly ash (Ash B), glass bead (Particle C), silica (Particle D), aluminum oxide (Particle E), and calcium oxide (Particle F), were used to study the charging characteristic of different particles. Among these particles, Ashes A and B mainly consisted of silica, aluminum oxide, iron oxide, calcium oxide, and magnesium oxide. The main components of Particles D, E, and F were silica, aluminum oxide, and calcium oxide, respectively. The mass concentration of Ash/Particle A, B, C, D, E, and F was approximately 196, 91, 48, 149, 394, and 139 mg cm^{-3}, respectively. The number concentration of Ash/Particle A, B, C, D, E, and F was approximately 182,489, 215,488, 208,578, 155,549, 210,959, and 233,843 # cm^{-3}, respectively. During the experiment the particle mass and number concentration varied slightly around the set value. The particle charging characteristics of different main components under the conditions of 0.1 s charging time and 30% relative humidity are shown in Fig. 7. The particle charge under the same applied voltage was ranked in the order of F > E > A > B > D > C. As indicated by other researchers (Chełkowski, 1980), the relative dielectric constant of Particles C, D, E, and F are 4.3–5, 4.5, 9, and 11.8, respectively. In addition, X-ray fluorescence is used to detect the elemental compositions of Ashes A and B. For Ashes A and B, the relative dielectric constant is calculated using Eq. (3) (Rao *et al.*, 2000):

$$\ln\varepsilon = \sum x_i\varepsilon_i \tag{3}$$

where x_i is the component i taking up the percentage of the particle, and ε_i is the relative dielectric constant of component i. The relative dielectric constant of all experimental ashes is shown in Table 1. The polarization capability of the particle with high relative dielectric constant is much stronger. Then, many more ions collided with the particle. Thus, the particle charging was enhanced. The particle charge under different applied voltages was investigated for clarification.
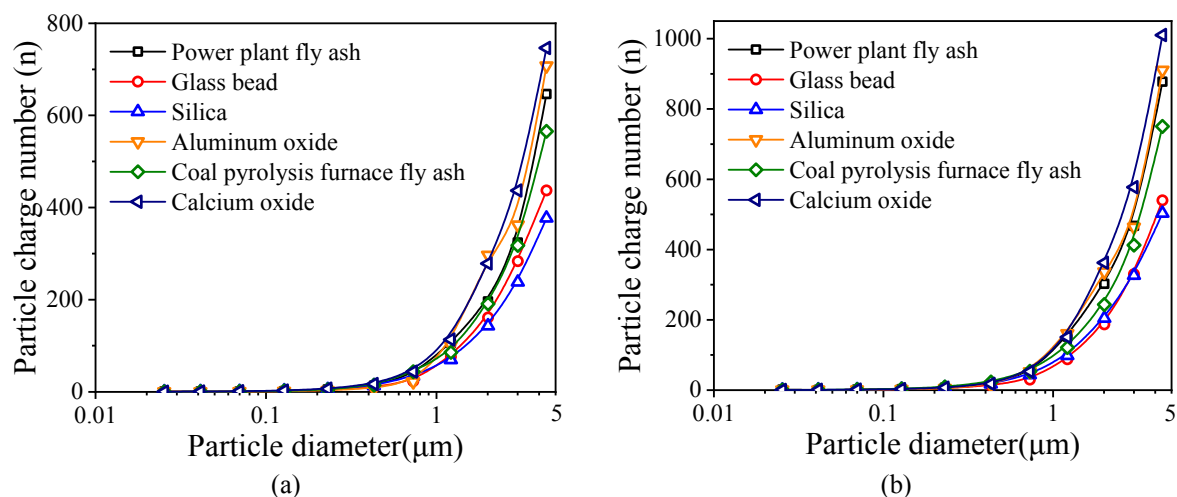
Fig. 7. Effect of main particle component on particle charge at different applied electric field strengths: (a) –4.2 kV cm^{-1}; (b) –5.0 kV cm^{-1}.

Table 1. Relative dielectric constant of experimental ash.

Type	F	E	A	B	C	D
Relative dielectric constant	11.8	9	6.8	6.4	4.3–5	4.5

At the same applied voltage, particle charge increased with the dielectric constant. In addition, the particle charge at the same size was ranked in the order of F > E > A > B > D > C, indicating that the difference in dielectric constant was the main reason for the evident change in charge for different types of particle. Therefore, the particle charge increased with the dielectric constant (Fig. 8). The particle charge was 377 e when the relative dielectric constant was 4.5 and increased to 746 e with increasing relative dielectric constant up to 11.8 at –4.2 kV cm^{-1}.

Effect of the Humidity in Flue Gas on Particle Charging
Fig. 9 reveals the effect of humidity on particle charge when the relative humidity is 10%, 30%, 60%, and 80%. The average applied electric field strengths are –4.2 and
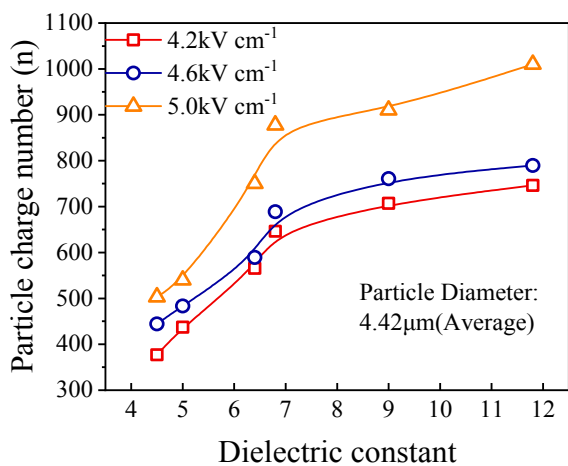

Fig. 8. Effect of dielectric constant on particle charge at different applied electric field strengths.

–5.0 kV cm^{-1}, the charging time is 0.1 s, and a ribbon electrode is used. The fly ash from a power plant was used as the experimental particle. For particles in the range of 0.1–10 µm, the particle charge increases with relative humidity under the same discharge voltage conditions. In addition, the enhancement of particle charge increased rapidly with the particle size (Fig. 9). Fig. 10 illustrates the effect of relative humidity on the charge of particle with diameters of 0.13, 0.23, 0.43 µm. For a particle, its charge increases with relative humidity. Increasing the relative humidity of the flue gas has a remarkable effect on the promotion of particle charge. For particles with sizes larger than 0.1 µm, the average charge was increased by more than 50% as the relative humidity increased from 30% to 80%. On the one hand, the ionization coefficient increased with relative humidity in the air, thereby leading to drastic ionization process of neutral molecules in corona discharge. Thus, the ion density was high, the number of negative ions that move to the low electrical field strength area of ESP is higher, and the probability of collision with particle increases. Then the current increased (as shown in Fig. 11). Finally, a high relative humidity promotes particle charge. On the other hand, particle absorbed water vapor in the air in a stable high-humidity environment. The vapor condensed on the surface of the particle, thereby increasing the water content of the particle. The relative dielectric constant of water, which is 80, is higher than that of the fly ash from the power plant (4–12). Therefore, compared with the completely dry particle, the polarization capability of the particle containing more water was very strong in the electric field, thereby allowing more electric field line to reach the surface of the particle. The collision between particles and ions was frequent. Thus, the particle charge was enhanced.
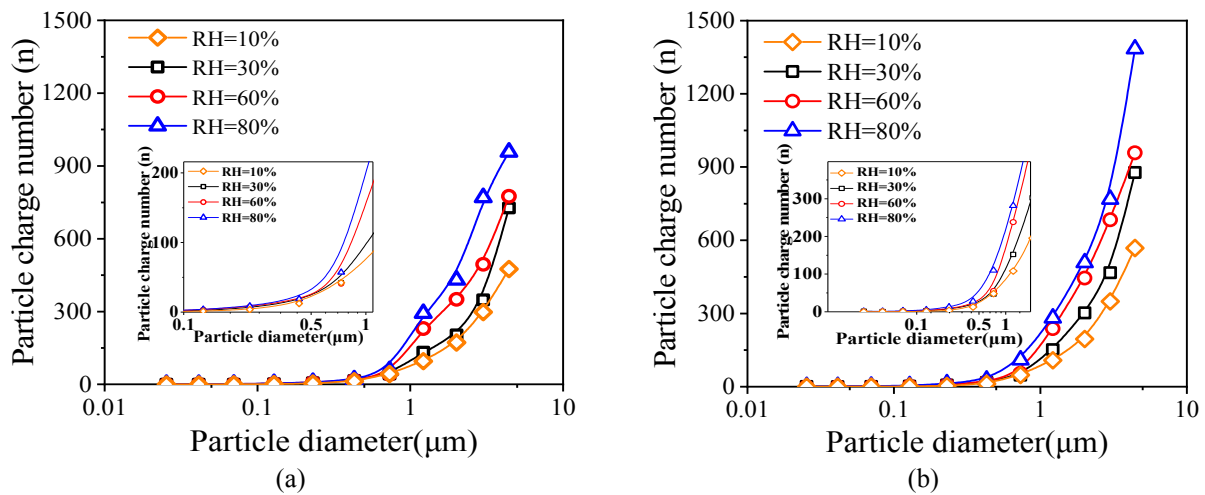
Fig. 9. Effect of relative humidity on particle charge at different applied electric field strengths: (a) –4.2 kV cm^{-1}; (b) –5.0 kV cm^{-1}.
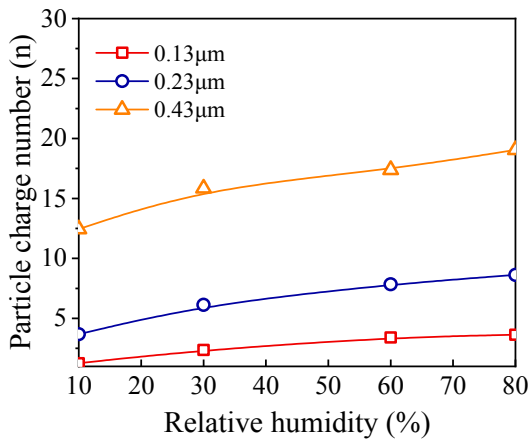

Fig. 10. Effect of relative humidity on particle charge with three different sizes.
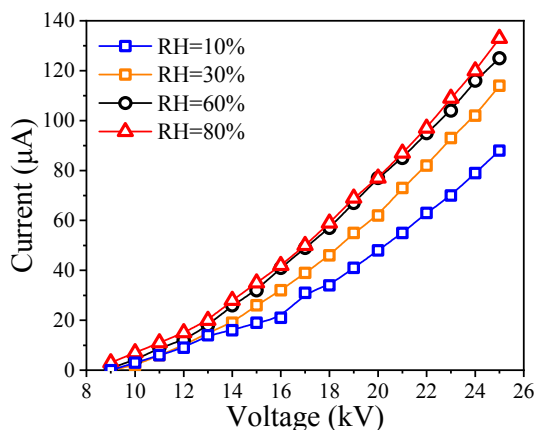

Fig. 11. I–V characteristics curve at different levels of humidity.

Optimization of the Selection of a Discharge Electrode

In this section, the effect of the electrode and current density on particle charge was studied. The corona current of different electrodes under the same applied voltage can be transformed into average current density by calculation. The current can be obtained by a current detecting device inside the power supply. The current density was calculated using Eq. (4) at the grounded plates:

$$J = I/A \qquad (4)$$

where J is the current density (mA m^{-2}), I is the current (mA), and A is the area of each grounded plate (m^2).

Fig. 12 reveals the effect of electrodes on particle charge when the relative humidity is 80%, the average applied electric field strength is –4.2 kV cm^{-1}, and the charging time is 0.1 s. In this research, five types of discharge electrodes, including ribbon, sawtooth, screw, and wire (d = 1, 3 mm), were examined to determine the performance of particle charging. The maximum particle charge for different electrodes is ranked in the same order as the maximum current density is ranked for different electrodes (Fig. 12). At the same applied voltage, the particle charge of the ribbon electrode was larger than that of the other four electrodes. When the electrode changed from wire electrode (d = 1 mm) to ribbon electrode, the particle charge significantly rose to more than 75% for a particle size of 0.7 μm. At the same voltage, optimizing the electrode form greatly promoted the current density in the precipitator (as shown in Fig. 13) and then increased ion density and enhanced particle charge. The effect of current density on particle charging is shown in Fig. 14. For a particle with the same size, the increase of the particle charge was positively correlated with the increase of current density. The ion density increased with the current density. The frequency of the collision between particle and ion increased, thereby resulting in the promotion of particle charge.

CONCLUSION

In this study, a particle charge measurement system was designed to study the effects of particle composition and
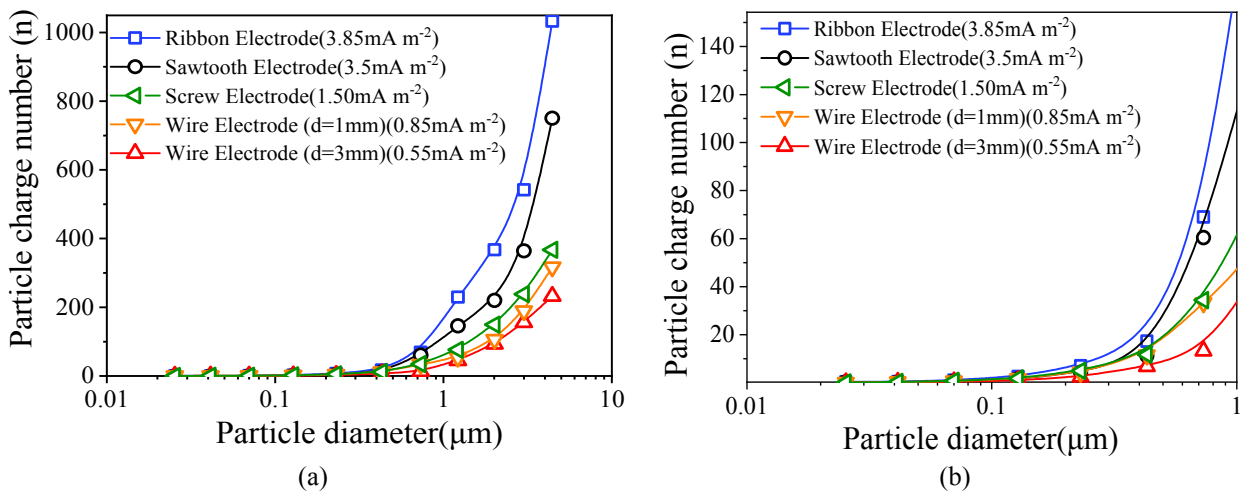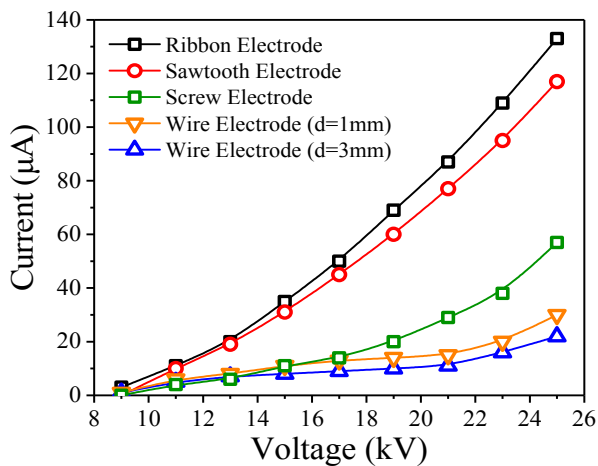
Fig. 12. Effect of electrodes on particle charge.

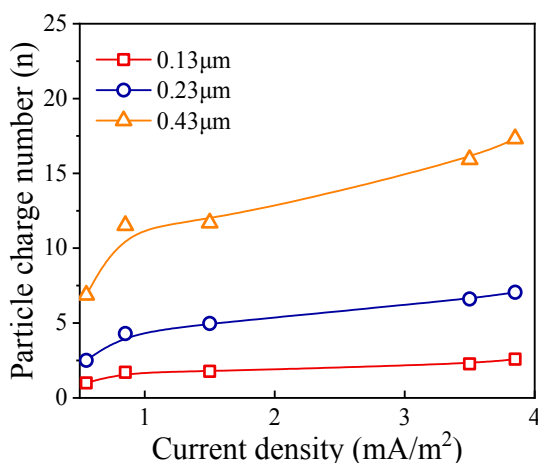**Fig. 13.** I–V characteristics curve at different electrodes.

Fig. 14. Effect of current density on particle charge with different sizes.

flue gas parameters on particle charging. Based on the results, we present a series of methods for enhancing charging. The following conclusions can be drawn:

(1) Increasing the temperature while maintaining the same applied electric field strength can enhance particle charging. In addition, when the applied electric field strength is high, this enhancement is rapid.

(2) Charging can be significantly enhanced by optimizing the particle composition and thereby increasing the relative dielectric constant. The particle charge is 377 *e* when the relative dielectric constant is 4.5; when the constant increases to 11.8 at –4.2 kV cm^{-1}, however, the charge increases to 746 *e*.

(3) High relative humidity promotes particle charging. The average charge of particles > 0.1 μm increased by more than 50% when the relative humidity rose from 30% to 80%.

(4) Particle charging is affected by the type of discharge electrode. The ribbon electrode, which discharges the largest current, is the optimal choice for particle charging, followed by the sawtooth, screw, and wire electrodes (d = 1 or 3 mm). With an electric field strength of – 4.2 kV cm^{-1}, the ribbon electrode produces a charge of 70 *e* for 0.7 μm particles, which is significantly higher than that of the other electrodes.

REFERENCES

Alonso, M. and Huang, C.H. (2015). High-efficiency electrical charger for nanoparticles. *J. Nanopart. Res.* 17: 332.

Biskos, G., Mastorakos, E. and Collings, N. (2004). Monte-Carlo simulation of unipolar diffusion charging for spherical and non-spherical particle. *J. Aerosol Sci.* 35: 707–730.

Chełkowski, A. (1980). *Dielectric physics*. Elsevier

Science & Technology.

Chien, C.L. and Tsai, C.J. (2013). Improvement of the nanoparticle charging efficiency of a single-wire corona unipolar charger by using radial sheath airflow: Numerical study. *Aerosol Sci. Technol.* 47: 417–426.

Chien, C.L., Tsai, C.J., Chen, H.L., Lin, G.Y. and Wu, J.S. (2011). Modeling and validation of nanoparticle charging efficiency of a single-wire corona unipolar charger. *Aerosol Sci. Technol.* 45: 1468–1479.

Crilley, L.R., Ayoko, G.A., Stelcer, E., Cohen, D.D., Mazaheri, M. and Morawska, L. (2014). Elemental composition of ambient fine particles in urban schools: Sources of children's exposure. *Aerosol Air Qual. Res.* 14: 1906–1916.

Domat, M., Kruis, F.E. and Fernandez-Diaz, J.M. (2014). Determination of the relevant charging parameters for the modeling of unipolar chargers. *J. Aerosol Sci.* 71: 16–28.

ExxonMobil (2017) Outlook for Energy http://www.ind iaenvironmentportal.org.in/files/file/2017_Outlook_For_ Energy.pdf.

Frank, G.P., Cederfelt, S.I. and Martinsson, B.G. (2004). Characterisation of a unipolar charger for droplet aerosols of 0.1–2.0 μm in diameter *J. Aerosol Sci.* 35: 117–134.

Ghaleb, F., Benstâali, W. and Belasri, A. (2008). Calculation of breakdown voltage in plasma display panels. *Mater. Sci. Eng., C* 28: 791–794.

Ghaleb, F. and Belasri, A. (2012). Numerical and theoretical calculation of breakdown voltage in the electrical discharge for rare gases. *Radiat. Eff. Defects Solids* 167: 377–383.

Gopalakrishnan, R., Thajudeen, T., Ouyang, H. and Hogan, C.J. (2013). The unipolar diffusion charging of arbitrary shaped aerosol particles. *J. Aerosol Sci.* 64: 60–80.

Hamou, N., Massinissa, A. and Youcef, Z. (2013). Modeling and simulation of the effect of pressure on the corona discharge for wire-plane configuration. *IEEE Trans. Dielectr. Electr. Insul.* 20: 1547–1553.

Hewitt, G.W. (1957). The charging of small particles for electrostatic precipitation. *Trans. Am. Inst. Electr. Eng. Part I* 76: 300–306.

Hu, W., Zhang, Y., Liu, S., Zheng, C., Gao, X., Nova, I. and Tronconi, E. (2017). Improvement in activity and alkali resistance of a novel V-Ce(SO$_4$)$_2$/Ti catalyst for selective catalytic reduction of NO with NH$_3$. *Appl. Catal., B* 206: 449–460.

Jaworek, A., Krupa, A. and Czech, T. (2007). Modern electrostatic devices and methods for exhaust gas cleaning: A brief review. *J. Electrostat.* 65: 133–155.

Kim, K.H., Kabir, E. and Kabir, S. (2015). A review on the human health impact of airborne particulate matter. *Environ. Int.* 74: 136–143.

Lawless, P.A. (1996). Particle charging bounds, symmetry relations, and an analytic charging rate model for the continuum regime. *J. Aerosol Sci.* 27: 191–215.

Li, X., Sun, W., Zhao, L. and Cai, J. (2019). Emission characterization of particulate matter in the ironmaking process. *Environ. Technol.* 40: 282–292.

Lin, N.H., Chang, M.B., Hwang, J., Kaneyasu, N. and Zhang, R. (2018). Overview of the special issue "Aerosol Source, Transport, Chemistry, and Emission Control" for the 10th Asian Aerosol Conference 2017. *Aerosol Air Qual. Res.* 18: 1515–1518.

Long, Z. and Yao, Q. (2010). Evaluation of various particle charging models for simulating particle dynamics in electrostatic precipitators. *J. Aerosol Sci.* 41: 702–718.

Park, J., Kim, C., Jeong, J., Lee, S.G. and Hwang, J. (2011). Design and evaluation of a unipolar aerosol charger to generate highly charged micron-sized aerosol particles. *J. Electrostat.* 69: 126–132.

Shin, W.G., Qi, C., Wang, J., Fissan, H. and Pui, D.Y.H. (2009). The effect of dielectric constant of materials on unipolar diffusion charging of nanoparticles. *J. Aerosol Sci.* 40: 463–468.

Sun, W., Liu, X., Xu, Y., Zhang, Y., Chen, D., Chen, Z. and Xu, M. (2018). Effects of the modified kaolin sorbents on the reduction of ultrafine particulate matter (PM$_{0.2}$) emissions during pulverized coal combustion. *Fuel* 215: 153–160.

Wang, C., Liu, X., Li, D., Si, J., Zhao, B. and Xu, M. (2015). Measurement of particulate matter and trace elements from a coal-fired power plant with electrostatic precipitators equipped the low temperature economizer. *Proc. Combust. Inst.* 35: 2793–2800.

Wang, W., Shao, L., Li, J., Chang, L., Zhang, D., Zhang, C. and Jiang, J. (2019). Characteristics of individual particles emitted from an experimental burning chamber with coal from the lung cancer area of Xuanwei, China. *Aerosol Air Qual. Res.* 19: 355–363.

Xu, F., Luo, Z., Bo, W., Zhao, L., Gao, X., Fang, M. and Cen, K. (2009). Experimental investigation on charging characteristics and penetration efficiency of PM$_{2.5}$ emitted from coal combustion enhanced by positive corona pulsed ESP. *J. Electrostat.* 67: 799–806.

Xu, Y., Liu, X., Cui, J., Chen, D., Xu, M., Pan, S., Zhang, K. and Gao, X. (2016a). Field measurements on the emission and removal of PM$_{2.5}$ from coal-fired power stations: 4. PM removal performance of wet electrostatic precipitators. *Energy Fuels* 30: 7465–7473.

Xu, Y., Liu, X., Zhang, Y., Sun, W., Zhou, Z., Xu, M., Pan, S. and Gao, X. (2016b). Field measurements on the emission and removal of PM$_{2.5}$ from coal-fired power stations: 3. direct comparison on the PM removal efficiency of electrostatic precipitators and fabric filters. *Energy Fuels* 30: 5930–5936.

Yang, R., Jianmin, Q., Marinis, T. and Wong, C.P. (2000). A precise numerical prediction of effective dielectric constant for polymer-ceramic composite based on effective-medium theory. *IEEE Trans. Compon. Packag. Technol.* 23: 680–683.

Yang, Z., Zheng, C., Zhang, X., Li, C., Wang, Y., Weng, W. and Gao, X. (2017). Sulfuric acid aerosol formation and collection by corona discharge in a wet electrostatic precipitator. *Energy Fuels* 31: 8400–8406.

Yang, Z., Zheng, C., Liu, S., Guo, Y., Liang, C., Zhang, X., Zhang, Y. and Gao, X. (2018a). Insights into the role of particle space charge effects in particle precipitation

processes in electrostatic precipitator. *Powder Technol.* 339: 606–614.

Yang, Z., Zheng, C., Zhang, X., Chang, Q., Weng, W., Wang, Y. and Gao, X. (2018b). Highly efficient removal of sulfuric acid aerosol by a combined wet electrostatic precipitator. *RSC Adv.* 8: 59–66.

Yang, Z., Zheng, C., Zhang, X., Zhou, H., Silva, A.A., Liu, C., Snyder, B., Wang, Y. and Gao, X. (2018c). Challenge of SO₃ removal by wet electrostatic precipitator under simulated flue gas with high SO₃ concentration. *Fuel* 217: 597–604.

Zheng, C., Chang, Q., Lu, Q., Yang, Z., Gao, X. and Cen, K. (2016). Developments in unipolar charging of airborne particles: Theories, simulations and measurements. *Aerosol Air Qual. Res.* 16: 3037–3054.

Zheng, C., Wang, Y., Zhang, X., Yang, Z., Liu, S., Guo, Y., Zhang, Y., Wang, Y. and Gao, X. (2018). Current density distribution and optimization of the collection electrodes of a honeycomb wet electrostatic precipitator. *RSC Adv.* 8: 30701–30711.

Zheng, C., Wang, Y., Liu, Y., Yang, Z., Qu, R., Ye, D., Liang, C., Liu, S. and Gao, X. (2019). Formation, transformation, measurement, and control of SO₃ in coal-fired power plants. *Fuel* 241: 327–346.

Zhou, B., Feng, L., Shiue, A., Hu, S.C., Wang, Y., Li, F., Lin, T., Liu, H.F., Wei, P. and Xu, Y. (2019). Study on influencing mechanism of outdoor plant-related particle on indoor environment and its control measures during transition period in Nanjing. *Aerosol Air Qual. Res.* 19: 571–586.

Zhuang, Y., Jin Kim, Y., Gyu Lee, T. and Biswas, P. (2000). Experimental and theoretical studies of ultra-fine particle behavior in electrostatic precipitators. *J. Electrostat.* 48: 245–260.